Science of the Total Environment 553 (2016) 474–485

Contents lists available at ScienceDirect

Science of the Total Environment

journal homepage: www.elsevier.com/locate/scitotenv

The effects of the built environment, traffic patterns, and micrometeorology on street level ultrafine particle concentrations at a block scale: Results from multiple urban sites

Wonsik Choi [a,b,*], Dilhara Ranasinghe [a], Karen Bunavage [a], J.R. DeShazo [c], Lisa Wu [c], Rodrigo Seguel [a,d], Arthur M. Winer [e], Suzanne E. Paulson [a,b]

[a] University of California, Los Angeles, Department of Atmospheric and Oceanic Sciences, 405 Hilgard Ave., Los Angeles, CA 90095, USA
[b] University of California, Los Angeles, Institute of the Environment and Sustainability, La Kretz Hall, Suite 300, Los Angeles, CA 90095, USA
[c] University of California, Los Angeles, Luskin Center for Innovation, Luskin School of Public Affairs, 3250 Public Affairs Bldg., Los Angeles, CA 90095, USA
[d] Center for Environmental Sciences, Faculty of Sciences, University of Chile, Las Palmeras 3425 Ñuñoa, Santiago, Chile
[e] University of California, Los Angeles, Fielding School of Public Health, Environmental Health Sciences Department, 650 Charles Young Dr., Los Angeles, CA 90095, USA

HIGHLIGHTS

- This study quantitatively examined built-environment effects on near-road UFP level.
- Block-scaled UFP conc. strongly depend on built environment and surface turbulence.
- Areal aspect ratio was a major contributor to UFP variations in the morning.
- Surface turbulence was a major contributor to UFP variations in the afternoon.
- Heterogeneous building morphology helps reduce UFP levels in the afternoon.

GRAPHICAL ABSTRACT

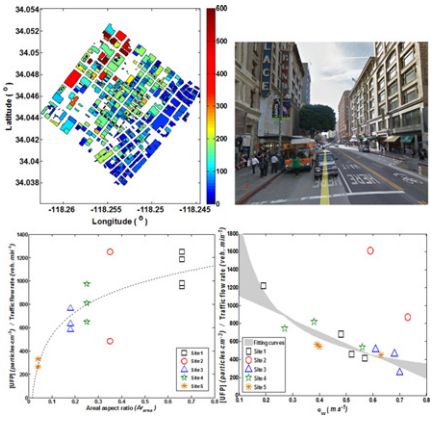

ARTICLE INFO

Article history:
Received 2 December 2015
Received in revised form 4 February 2016
Accepted 12 February 2016
Available online 22 March 2016

Editor: D. Barcelo

Keywords:
Ultrafine particles
Built-environment
Aspect ratio

ABSTRACT

This study attempts to explain explicitly the direct and quantitative effects of complicated urban built-environment on near-road dispersion and levels of vehicular emissions at the scale of several city blocks, based on ultrafine particle concentrations ([UFP]). On short timescales, ultrafine particles are an excellent proxy for other roadway emissions. Five measurement sites in the greater Los Angeles with different built environments but similar mesoscale meteorology were explored. After controlling for traffic, for most sampling days and sites, morning [UFP] were higher than those in the afternoon due to limited dispersion capacity combined with a relatively stable surface layer. [UFP] at the intersection corners were also higher than those over the sampling sites, implying that accelerating vehicles around the intersections contributed to [UFP] elevation. In the calm morning, the areal aspect ratio (Ar_{area}), developed in this study for real urban configurations, showed a strong relationship with block-scale [UFP]. Ar_{area} includes the building area-weighted building height, the amount of open space, and the building footprint. In the afternoon, however, when wind speeds were generally

* Corresponding author at: Pukyong National University, Geo-Science Institute, 45 Yongso-ro, Nam-gu, Busan, Republic of Korea.
E-mail address: wschoi@atmos.ucla.edu (W. Choi).

http://dx.doi.org/10.1016/j.scitotenv.2016.02.083

Turbulence
Pedestrian exposure
Transit-oriented development

higher and turbulence was stronger, vertical turbulence intensity σ_w was the most effective factor controlling [UFP]. The surrounding built environment appears to play an indirect role in observed [UFP], by affecting surface level micrometeorology. The effects are substantial; controlling for traffic, differences in Ar_{area} and building heterogeneity were related to differences in [UFP] of factors of two to three among our five study sites. These results have significant implications for pedestrian exposure as well as transit-oriented urban planning.

1. Introduction

Vehicle emissions are rapidly diluted away from roadways, thus leading to highly spatially-heterogeneous pollutant concentrations in urban areas. A large fraction of the exposure of many individuals to many pollutants can be attributed to relatively short periods of time spent on and near roadways, which often have highly elevated pollutant concentrations compared to areas at even moderate distances from roadways (Behrentz et al., 2005; Fruin et al., 2004; Marshall et al., 2005; Morawska et al., 2008). However, because of the lack of adequate pollutant measurement data near roadways, studies of health effects attributed to transportation-related air pollutants have generally used freeway or arterial roadway proximity as a proxy for vehicle-related air pollution (Brugge et al., 2007; Ren et al., 2008; Volk et al., 2011; Zhou and Levy, 2007). Despite this rather blunt approach, near roadway pollution studies have shown moderate increases in a long list of adverse health outcomes, including increased incidence of cancer (Pearson et al., 2000), asthma (Janssen et al., 2003), general mortality (Hoek et al., 2002), heart attacks (Tonne et al., 2007), autism (Volk et al., 2011), pre-term birth (Ren et al., 2008) and other adverse outcomes associated with proximity to roadways.

Of a wide range of particle- and gas-phase species contained in fresh vehicular emissions, ultrafine particles (UFP; particles smaller than 100 nm in diameter) are one of the best tracers of near-roadway pollution, due to their large dynamic concentration ranges (10^3 to 10^6 particles$\cdot$cm^{-3}) and relatively short life time, which results in low and steady background concentrations (Capaldo and Pandis, 2001; Choi et al., 2013), and the availability of high time resolution (1 s) instrumentation that allows resolution of pollutant gradients controlled by complex dispersion.

Despite an increasing amount of literature related to near-roadway exposures, surprisingly little is known about how to proactively design and plan for these transit environments in order to minimize air pollution exposures. Therefore, it is desirable to develop a set of comprehensive recommendations on how to reduce pedestrian and residential air pollution exposures that will aid transportation and urban planners make future development plans. These may include traffic controls and urban building configuration, which impact emissions and dispersion, respectively. Within the transit environment, urban planners also decide spatially where pedestrian density will be greatest through their choices of where to site transit stops, sidewalks, and parks.

Several studies investigating the influence of the built environment on street level concentrations have been published recently, mostly focusing on deep street canyons and a few others. Four recent studies have taken the first step towards understanding dispersion of traffic-related pollutants in urban areas with inhomogeneous building morphology, which is our focus (Boarnet et al., 2011; Boogaard et al., 2011; Buonanno et al., 2011; Pirjola et al., 2012). Buonanno et al. (2011) focused on particles, including UFP, measured in four different street canyons with different building height-to-street width ratios (H/W = 0.5 to 1.3) in a town in central Italy; Pirjola et al. (2012) investigated dispersion of traffic emissions (focusing on UFP) in three different micro-environments (but with similar H/W ~ 0.5) in Helsinki, Finland; Boogaard et al. (2011) conducted an extensive study in the Netherlands in which five species, including particle number concentrations and black carbon, were measured over 6 weeks at 8 urban roadside locations in five cities; and Boarnet et al. (2011) examined the factors governing $PM_{2.5}$ measured on sidewalks next to arterial roadways in five cities in southern California.

Of these studies, Boogaard et al. (2011) and Boarnet et al. (2011) conducted stationary measurements of roadway pollutants, whereas Buonanno et al. (2011) and Pirjola et al. (2012) used a mobile platform to characterize UFP concentrations with a high temporal resolution. Boogaard et al. (2011) reported the two streets with buildings lining one or both sides of the streets showed the largest road contributions although their results did not discern the roles of meteorology, detailed building morphologies, and emissions. Boarnet et al. (2011) suggested the most effective controlling factors for sidewalk $PM_{2.5}$ concentrations are daily variations, time of day, winds, and temperature. They also argued that traffic and built environment variables accounted for only a small amount of variation, although they are statistically significant. However, their built environment variables were classified rather than quantified. After accounting for these most effective controlling factors, they concluded that street canyons with higher than 5-story buildings are related to high $PM_{2.5}$ concentrations, and adjacent paved lots were negatively associated with concentrations. Buonanno et al. (2011) and Pirjola et al. (2012) using mobile platform measurements, concluded that the surrounding built environment significantly affects pollutant concentrations in urban microenvironments by changing the dispersion. However, both studies considered only the averaged H/W and did not consider the detailed information of built environment such as the gaps between buildings and open spaces if any, and also did not quantitatively examine the role of built environment in pollutant concentrations.

While these studies provide insight into air pollution in built environments, the measurements lack the spatial resolution and completeness to discern contributions of detailed urban morphology and traffic control at a level that might inform highly-local planning decisions about the built environment and traffic flow regimes. Minimizing exposure to transportation-related air pollution is not fully considered currently in the process of planning for transit-oriented developments (TOD) (Haughey and Sherriff, 2010).

There are several relevant spatial scales to the investigation of the built environment with pollutant concentrations. Here we focus on a spatial scale of several city blocks. We develop quantitative links among the variables that control dispersion in complex urban environments, including building morphology, traffic flow rates, and micrometeorology. We consider data from five sites in the greater Los Angeles area, each with similar fleet composition and synoptic meteorology, but markedly different built environments and traffic flow patterns. Measurements were performed in both the early morning and mid-afternoon, which have significantly different atmospheric stability and wind profiles.

2. Methods

2.1. Sampling sites and built-environmental characteristics

Extensive field experiments, including mobile and stationary measurements of vehicular pollutants and traffic, were conducted at four sites in and around downtown Los Angeles (DTLA) and at a site in Temple City, located 20 km east of DTLA, for 16 days between July and November of 2013 (Fig. S1; Table 1). Each sampling site represents a distinct urban built environment with a different building morphology

Table 1
Description of field measurements including built-environments, measurement dates, instrumentation, and sampling design.

Sites	Built-env.	Date	Instrumentation	Sampling strategy
Broadway & 7th St.	Street canyon with tall buildings (H > 40 m)	7/1	[1] ARB-MMP; 2 DM; 2 sonic towers (roof &	[A] 2 DM were paired across the street, staying
Site1	at both side of the street.	7/2	surface); 4 traffic recording cameras	about 5 min at mid-blocks and intersections
	Highly trafficked on both streets.	7/3		(quasi-stationary)
		7/5		
		11/13	[2] Lite-MMP; 3 DM; CPC; OPS; 2 surface	[B] 2 DM were stationary at the intersections
			sonic towers; 4 traffic cams	1 CPC & OPS stayed at the sonic tower
				1 DM stationary across the sonic tower
Temple City & Las Tunas	All short buildings (H < 6 m) around the	8/6	[1] but 1 sonic tower	[A]
Site5	site.	9/17	[3] Lite-MMP; 1 DM; CPC; OPS; 2 sonic	[C] 1 DM at intersection (staying 5 light cycles at
	Moderately trafficked	9/18	towers (roof & surface); 4 traffic cameras	each corner) and CPC & OPS stayed next to sonic
	(Las Tunas > Temple).			tower
Olive & 12th St.	One tall building at one corner of	9/24	[3]	[C]
Site2	intersection + many open space.	9/25		[C] but 1 DM was stationary across the sonic
	Sparse traffic.			tower
Vermont & 7th St.	One tall building at intersection.	10/7	[3]	[C]
Site3	Large traffic on Vermont.	10/14		
		11/18	[2]	[B]
Wilshire & Carondelet	Two tall buildings.	11/1	[2]	[A] and additional DM was stationary across the
Site4	Modest traffic on Wilshire.			sonic tower
		11/6	[2]	[B]
		11/20	[2]	[B]

ARB-MMP: California Air Resources Board mobile monitoring platform, Lite-MMP: electric vehicle equipped with a DiSCmini, DM: DiSCmini ultrafine particle counter, CPC: condensation particle counter, and OPS: optical particle size.

(e.g., building heights and areas, intersection areas, street widths, building densities and homogeneity) and traffic patterns (e.g. flow rates, traffic densities, fleet compositions, traffic light cycle periods). Each sampling site covered a 2-by-2 (or 3) block area centered on a main intersection where stationary sampling of pollutants and traffic monitoring were conducted, depending on availability of instruments. All sites were located more than 800 m from the nearest freeway, well outside the range of freeway influence during daytime. As UFP are relatively short lived and upwind areas for all sites consist of similarly developed urban areas for many kilometers, the influence of areas farther than the neighbouring several streets are not expected to be discernable in this dataset.

The Broadway and 7th St. site (*Site1*) located in DTLA (34.04519°N/118.25639°W) is a street canyon environment surrounded by tall commercial buildings on both sides of the streets. Building heights were >40 m with little, if any, gaps between buildings. The block lengths/street widths (measured from building face to building face on the two sides of the street) of Broadway and 7th streets are 190 m/26 m and 100 m/22 m, respectively (Table 2). The Olive and 12th St. site (*Site2*) is located 1 km southeast of *Site1* (34.03943°N/118.26226°W). The intersection is occupied by a 130 m tall isolated skyscraper surrounded by large open spaces and low-story buildings. This site had low traffic flows and short queues. The block lengths/street widths of Olive and 12th St. are 180 m/28 m and 95 m/17 m, respectively. The Vermont and 7th St. site (*Site3*) located 4 km northwest of *Site1* (34.05976°N/118.29164°W) is similar to the *Site2*, but surrounding buildings are more densely patched and open spaces are smaller. In addition, Vermont Ave. in *Site3* is one of the busiest arterials in the Los Angeles area. The block lengths/street widths of Vermont Ave. and 7th St. are 190 m/30 m and 95 m/25 m, respectively. The Wilshire and Carondelet St. site (medium-sized buildings on one side, *Site4*) is located 3 km northwest from *Site1* and 1 km east from *Site3* (34.06012°N/118.28054°W). *Site4* represents a typical city environment in the Los Angeles area, consisting of a mixture of open space and moderately-sized buildings. The whole block of the south side of Wilshire Blvd. is occupied by 30 m and 50 m tall buildings while the north side is open or occupied by 5 or 10 m tall buildings. The block lengths/street widths of *Site4* are 75 m/37 m (Wilshire) and 160 m/17 m (Carondelet). Finally, the Temple City and Las Tunas Blvd. site (a low and flat residential site, *Site5*) in Temple City (34.10669°N/118.06090°W) is surrounded mostly by one-story single family homes and small commercial buildings (<6 m in height). The block lengths/street widths of Temple City and Las Tunas Blvd. are 175 m/24 m and 115 m/30 m, respectively.

The sites are numerically ordered based on the height of urban canopy (mean building area-weighted building heights); lower numbers indicate higher building morphology; e.g., *Site1* has a street canyon and tall buildings; *Site5* has a low/flat urban configuration (Table 2). The distributions of buildings and building morphology around

Table 2
Built environments in the mobile sampling areas.

	Broadway & 7th (*Site1*)	Olive St. & 12th St. (*Site2*)	Vermont & 7th St. (*Site3*)	Wilshire & Carondelet (*Site4*)	Temple City & Las Tunas (*Site5*)
# of buildings	59	34	90	44	143
Max. building height (m)	58	129	80	57	8
Mean building height, H_{bldg} (m)	34	21	11	18	5
Bldg. area weighted height, H_{area} (m)	40	42	25	24	6
Bldg. homogeneity, H_{area}/H_{bldg} (dimensionless) (1 = perfectly homogeneous)	1.16	2.01	2.21	1.39	1.09
Mean building ground area (m^2)	1030	1395	585	992	225
Street width (m)	26 (BW)/22 (7th)	28 (Olive)/17 (12th)	30 (Ver)/25 (7th)	17 (Car)/37 (Wil)	24 (TC)/30 (LT)
Simple aspect ratio (H_{area}/W_{street})	1.7	1.9	0.9	0.9	0.2
Block length (m)	190 (BW)/100 (7th)	180 (Olive)/95 (12th)	190 (Ver)/95 (7th)	160 (Car)/75 (Wil)	175 (TC)/115 (LT)
Ratio occupied by bldg.	0.72	0.42	0.33	0.46	0.30

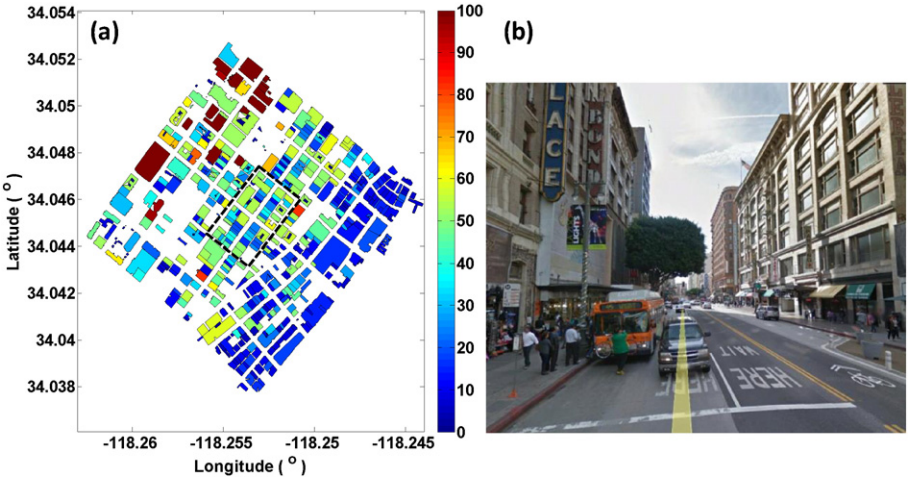

Fig. 1. (a) Map of building heights and morphology in downtown Los Angeles. Dashed black line shows the sampling area centered by the Broadway St. (Northeast-Southwest direction) & 7th St. intersection. Color bar represents the building heights in meters. (b) The street view on Broadway St. captured in Google Earth. The building distributions and street views for the other sites are presented in Supplementary information, Fig. S2.

sampling sites are presented in Supplementary information (SI) (Figs. 1 and S2 and Table 2).

2.2. Instrumentation and sampling design

A fully-equipped Toyota RAV4 electric sub-SUV, maintained by the California Air Resources Board (CARB), served as a mobile monitoring platform (ARB-MMP). A suite of fast response instruments in the ARB-MMP measures various air pollutants with 1 s temporal resolution, including UFP number concentrations (TSI, CPC 3007) and size distributions (TSI, FMPS 3009), nitrogen oxides (NOx) (Teledyne, API 200E), carbon monoxide (CO) (Teledyne, API 300E), carbon dioxide (CO_2) (LI-COR, LI-820), particle-bound polycyclic aromatic hydrocarbons (PB-PAH) (EcoChem PAS 2000), particulate matter with aerodynamic diameters < 2.5 μm ($PM_{2.5}$) (TSI DustTrak 8520), and black carbon (BC) (Magee Scientific Aethalometer). The ARB-MMP has been used in a series of near/on road air quality studies and detailed information is found elsewhere (Choi et al., 2012; Choi et al., 2013; Hu et al., 2012; Kozawa et al., 2009, and others). When the ARB-MMP was not available due to maintenance, an electric vehicle (Chevrolet Volt or Nissan Leaf) equipped with a DiSCmini was used instead. The DiSCmini is a fast diffusion size classifier that measures UFP number concentration (20–700 nm size range) and the mean size of UFP collected every second. Many of the measurements were performed with a DiSCmini hand held particle counter (Matter Aerosol AG).

As this instrument is relatively new, evaluations are only available for laboratory-generated nanoparticles under controlled indoor conditions (Bau et al., 2015; Mills et al., 2013). We provide additional inter-comparison data for our urban conditions. Briefly, for about 5–10 min before and after the measurements of all sessions (A.M. and P.M.), all particle number counters (4 DiSCminis and a CPC) were placed at the same location near roadways for inter-comparison under various atmospheric conditions. All five particle instruments were very stable over time; while there were some moderate deviations from 1:1 slopes (due to the individual instruments and /or the inlet tubing). The slopes were not observed to drift over time. The readings from all instruments agreed consistently within ca. 20% with excellent linearities ($R^2 \approx 0.9$ or better; see SI 2). Due to the upper limit of detection of CPC (10-^{5} particles·cm^{-3}), the comparison between CPC and DiSCmini was made with [UFP] < 8×10^4 particles·cm^{-3} (which excludes <4% of the total dataset; SI 2.3). An inlet tube (1.5 m long Tygon tubing supplied by provider) installed on the DiSCmini caused a 2 s delay (easily corrected), and diffusional and electrostatic particle losses due to the inlet tubing was estimated as 15% (SI 2.1). A comparison of the mean particle diameter between Scanning Mobility Particle Sizer (SMPS, TSI 3080) and DiSCmini was made separately on a rooftop at UCLA with an ambient air and showed perfect agreement and good linearity (with a slope of 1.00 and $R^2 = 0.67$; SI 2.4). In this study, all DiSCmini data were converted to corresponding CPC values based on the slopes of 1:1 comparisons (Eqs. (S1)–(S4)) so that the measured [UFP] can be compared directly because the CPC has been more widely and conventionally used in UFP air pollution studies. Detailed inter-comparison results are presented in SI 2.

In all cases, the inlet for instruments was located on the passenger side of the vehicle near the roofline (about 1.5 m height from the ground, matching the height of the pedestrians breathing zone), in as close proximity to the sidewalk as practical (roughly within 2–5 m). Thus, the concentrations measured by the MMP closely reflect the pedestrian exposure levels near the roadways. The same post-data processes described in Choi et al. (2012) were performed to synchronize instruments and precisely account for the response time (a time-lag correlation method on a twice-daily basis).

A GPS (GPSMAP 76CS, Garmin or BT-Q1000XT, Qstarz International Co., Ltd., depending on availability) was employed to record MMP positions every second, and the corrections of the GPS data were made using a line reference technique as described in detail in a companion paper (Ranasinghe et al., 2016). In this study, however, site-by-site comparisons are the main focus, and thus the highly spatially resolved data of the MMP were not used.

A combination of mobile and stationary measurements was conducted depending on the availability of instruments (Table 1). Intensive measurements were conducted for ~2 h twice a day, once in the early morning (06:00–09:00) and once in mid-afternoon (13:00–17:00). These periods represent two distinct meteorological conditions: limited mixing in the mornings vs. vigorous vertical mixing due to surface heating in the afternoons. A schematic of the sampling design is shown in Fig. 2. For the entire sampling period, the MMP drove four-leaf clover shaped routes around the main intersection, typically completing 7–12 repeats of the route for each morning or afternoon.

To supplement mobile measurements, a pair of UFP counters (DiSCmini) was deployed on pedestrian sidewalks. The DiSCmini pair, being positioned across the street from one another, sampled for 5–10 min at the mid-blocks and intersections on one street and then moved to other mid-block or intersection locations (Fig. 2). The objective of mobile sampling was to obtain highly resolved spatial distributions of pollutant concentrations, whereas paired measurements of UFP are useful for investigating street canyon and other effects caused by in-canopy circulation in different built environments. Also, paired

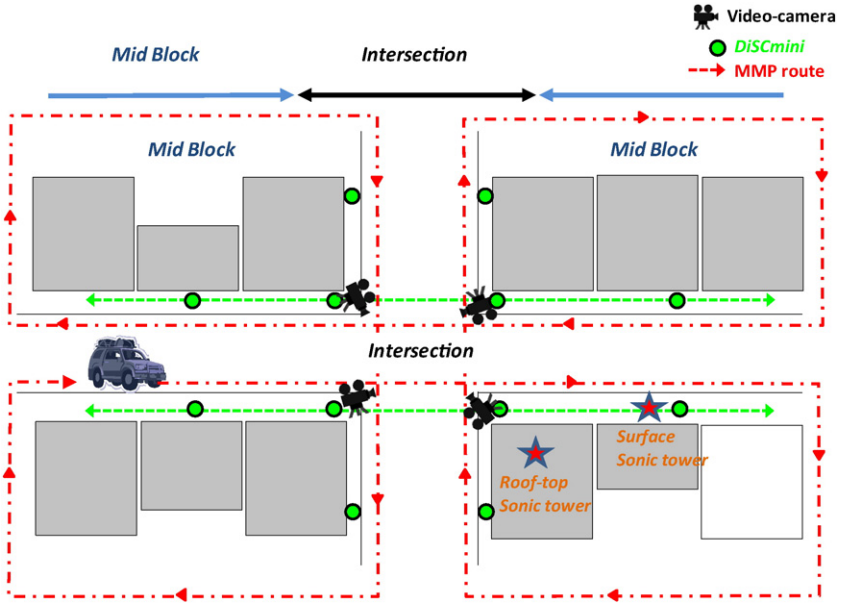

Fig. 2. A schematic of the intersection sampling design. Green circles denote the location of a DiSCmini pair (across the street) for 5-minute stationary measurements. Red stars represent the location of surface and roof-top (only when roof-top access was possible) sonic towers. The actual positions and spatial scales are different from this illustration.

DiSCmini measurements were taken in the immediate location of pedestrians at a height near breathing zones and therefore sampled direct pedestrian exposure to vehicular emissions.

2.3. Meteorological, traffic and built-environment parameters

Surface meteorological data were obtained from three-axis sonic anemometers (10 Hz CSAT3, Campbell Sci. Inc. and 21 Hz WindMaster, Gill Instruments Ltd.) installed on pedestrian sidewalks, 3 m above the ground level. Although we cannot separate vehicle-induced turbulence and building effects from ambient turbulence, the surface meteorological and micrometeorological information obtained here indicate the overall meteorological conditions within the building canopies in urban environments. Considered surface micrometeorological parameters include the mean wind speed, wind direction, friction velocity, three-directional wind fluctuations (σ_u, σ_v, and σ_w), and turbulence kinetic energy. The detailed procedure for calculating these micrometeorological parameters is presented in SI 3.

Building information, including building area, height, and location, was extracted from LARIAC2 Geographic Information System data (LARIAC, 2009). Because the scope of this study was to compare pollutant levels site-by-site with various collective characteristics of built environments, we additionally derived the customized building parameters at sampling area scale from GIS building information, including building-area-weighted building height, building density, heterogeneity and areal aspect ratio. The quantified built-environmental parameters for each sampling site are discussed in more detail in Section 3.3.

At the four corners of each central intersection (Fig. 2), directional traffic (north-, south-, east-, and west-bound) and traffic light signal status were recorded with four video cameras to provide highly detailed traffic information for the sampling periods. Traffic video files were reviewed and coded for the traffic parameters at 1 second resolution. The traffic parameters are: traffic light status (red, green, yellow), the number of passenger vehicles, heavy/medium duty vehicles and buses passing the central intersection, and the number of each type of vehicle waiting in queues during red lights. The 1-second resolution traffic data were used in a high resolution statistical model and will be presented in the separate publication. In the present study, the average period of traffic light cycles (P_{TL}), mean traffic flow rates for a P_{TL} (cars·min^{-1}), and mean number of cars in a queue (L_{que}) were calculated from the high resolution traffic codes and compared with the variations in UFP number concentrations of the five sampling sites.

3. Determination of characteristics of traffic, meteorology, and built environments

3.1. Traffic

Observed traffic characteristics at each site are shown in Table 3. The basic traffic light periods were 69 or 89 s; these changed actively depending on traffic conditions. Traffic rates (vehicles·min^{-1}) were comparable or higher in the afternoon sessions compared to morning sessions, except at *Site2*. The highest traffic rates were observed at *Site3* and *Site5* in both the mornings and afternoons. Although the traffic rates were comparable between *Site3* and *Site5*, traffic density at *Site3* was significantly higher due to unequal distributions of traffic between the two streets and the denser arterial-street-network in this commercial/business district. Of the five sampling sites, *Site1* and *Site5* had equal traffic between North-South and East-West streets and *Site3* and *Site4* showed significant disparity in traffic rates between N-S and E-W streets. *Site2* also had unequal traffic distributions, but the overall traffic rate was minimal for the whole day. Heavy- and medium-duty (HD and MD) vehicles were encountered infrequently for all sampling sites (<~1.5 vehicles·min^{-1}). Thus, for all study areas, gasoline vehicles were dominant, accounting for 95–98% of the total traffic rates except one case (for the afternoon on 9/25/2013, gasoline vehicles accounted for 90% of traffic rate due to very few passenger vehicles at this time and location). Based on consistent fleet compositions for the entire sampling sites and infrequent HD and MD traffic rates, we do not separate a fleet composition in further discussion. We feel that to attempt to account for slight differences in fleet composition between the sites would only introduce more errors, particularly because at the time of the field study the emissions from the HDDT fleet were changing rapidly due to a suite of new regulations. Further, observationally the fleet composition between these sites in terms of vehicle makers, models, and years was similar. Data from a more affluent area were not included in this study partly because of this issue, although the dominant factor in that decision was that the sampling route design was substantially different.

Table 3
Characteristic traffic patterns observed for each site for measurement periods. Values in parentheses are standard deviations.

Date	Morning					Afternoon				
	Light cycle s	Traffic rate #/min	HDV/MDV #/cycle	Queue length #/cycle	Traffic ratio	Light cycle s	Traffic rate #/min	HDV/MDV #/cycle	Queue length #/cycle	Traffic ratio
Site1 (street canyon)										
7/1	69 (4)	29 (2)	1.4 (1.2)	20 (5)	0.47					
7/2						89 (4)	41 (8)	0.9 (0.9)	31 (8)	0.51
7/3	69 (5)	29 (6)	1.0 (1.2)	18 (5)	0.44	89 (3)	43 (8)	0.9 (0.9)	29 (5)	0.52
7/5	70 (4)	22 (5)	0.9 (1.1)	12 (4)	0.48	89 (4)	35 (5)	0.5 (0.9)	29 (6)	0.49
11/13	69 (2)	34 (5)	0.9 (1.0)	21 (5)	0.56	69 (1)	28 (5)	1.4 (1.2)	20 (5)	0.47
Site2 (isolated skyscraper with low traffic rates)										
9/24	69 (2)	22 (7)	0.6 (0.8)	3 (2)	0.81	77 (10)	12 (3)	0.6 (0.6)	2 (1)	0.75
9/25	69 (3)	27 (7)	0.9 (0.9)	6 (3)	0.87	69 (1)	10 (3)	1.0 (0.7)	3 (2)	0.75
Site3 (isolated skyscrapers with high traffic rates)										
10/7	89 (3)	47 (6)	2.0 (1.2)	22 (6)	0.81	89 (1)	51 (7)	1.4 (1.1)	28 (6)	0.75
10/14	91 (12)	47 (7)	1.4 (1.1)	27 (7)	0.81	90 (11)	47 (6)	1.2 (1.0)	27 (7)	0.77
11/18	89 (1)	54 (7)	1.6 (1.1)	33 (7)	0.77	89 (2)	51 (6)	1.1 (1.0)	29 (6)	0.76
Site4 (one-side medium height buildings)										
11/1	110 (44)	30 (5)	1.2 (1.3)	4 (2)	0.95	98 (34)	29 (9)	1.0 (0.9)	5 (2)	0.94
11/6	100 (30)	35 (6)	0.8 (0.9)	4 (2)	0.93	107 (36)	29 (4)	0.8 (0.9)	6 (3)	0.92
11/20	100 (30)	35 (6)	0.9 (0.9)	5 (3)	0.91	97 (23)	30 (5)	1.1 (1.0)	6 (2)	0.89
Site5 (low and flat)										
8/6	71 (6)	45 (7)	1.7 (1.9)	24 (9)	0.44	79 (9)	64 (10)	1.2 (1.1)	50 (15)	0.48
9/17						70 (8)	49 (10)	1.6 (1.5)	27 (8)	0.46
9/18	81 (8)	61 (10)	1.8 (1.6)	41 (13)	0.49	69 (1)	55 (9)	1.4 (1.1)	33 (10)	0.48

3.2. Meteorology

Observed meteorology including detailed surface micrometeorology is summarized in Table 4 and Fig. S7 in SI 3. Morning meteorology was generally calm for all sampling sites, with mean wind speeds below 1.4 $m \cdot s^{-1}$ with 1σ values within 0.4 $m \cdot s^{-1}$; with the exception of 9/25/2013 at *Site2*, where the wind was exceptionally strong at 1.9 (±0.6) $m \cdot s^{-1}$. Friction velocity (u_*), vertical wind fluctuation (σ_w), and turbulence kinetic energy (TKE) appeared to be similar among the sites in the morning (Table 4). In the afternoon, wind speeds increased up to 3.3 $m \cdot s^{-1}$ with 1σ values within 0.6 $m \cdot s^{-1}$. Thus, meteorological conditions were not variable for 2-hour sampling periods. Turbulence parameters for afternoon sampling periods varied more widely between sites. For instance *Site1*, *Site4*, and *Site5* had a less turbulent surface atmosphere than *Site2* and *Site3*. As noted earlier *Site2* and *Site3* have more heterogeneous building morphology with one or two

Table 4
Surface micrometeorological conditions observed for sampling periods. Values in parentheses of the temperature and wind speed columns represent standard deviations.

Date	Morning					Afternoon				
	Temp. (°C)	Wind speed[a] m/s	u_* m/s	σ_w m/s	TKE $m^2 s^{-2}$	Temp. (°C)	Wind speed[a] m/s	u_* m/s	σ_w m/s	TKE $m^2 s^{-2}$
Site1 (street canyon)										
7/1	25.9 (±1.7)	1.0 (±0.2)	0.23	0.37	0.47	32.2 (±2.1)	1.1 (±0.3)	0.23	0.40	0.46
7/2	26.1 (±1.4)	1.2 (±0.3)	0.27	0.40	0.61	23.5 (±1.2)	1.7 (±0.3)	0.29	0.52	1.02
7/3	23.0 (±1.3)	1.2 (±0.1)	0.17	0.35	0.47	22.5 (±1.0)	1.7 (±0.2)	0.36	0.57	0.97
7/5	20.6 (±1.4)	0.9 (±0.2)	0.19	0.30	0.47	24.0 (±0.6)	1.6 (±0.2)	0.15	0.48	1.21
11/13	24.2 (±0.4)	0.8 (±0.2)	0.20	0.27	0.18	29.9 (±0.6)	0.5 (±0.1)	0.12	0.19	0.08
Site2 (isolated skyscraper with low traffic rates)										
9/24	26.6 (±0.4)	0.8 (±0.2)	0.15	0.24	0.23	28.3 (±0.2)	2.1 (±0.6)	0.72	0.73	1.90
9/25	21.7 (±0.5)	1.9 (±0.6)	0.88	0.97	1.83	24.9 (±0.4)	3.3 (±0.4)	0.48	0.59	1.84
Site3 (isolated skyscrapers with high traffic rates)										
10/7	22.8 (±0.5)	1.4 (±0.4)	0.13	0.41	0.77	27.8 (±0.7)	2.6 (±0.5)	0.40	0.68	2.11
10/14	17.9 (±1.4)	0.7 (±0.1)	0.35	0.38	0.31	28.6 (±0.4)	1.9 (±0.3)	0.42	0.61	1.26
11/18	15.4 (±0.4)	0.9 (±0.2)	0.23	0.36	0.39	20.2 (±0.4)	2.6 (±0.3)	0.27	0.70	1.60
Site4 (one-side medium height buildings)										
11/1	17.2 (±1.7)	1.2 (±0.4)	0.16	0.39	0.54	29.1 (±0.4)	0.9 (±0.2)	0.43	0.56	0.51
11/6	15.1 (±1.4)	0.9 (±0.1)	0.20	0.37	0.35	26.3 (±0.3)	0.6 (±0.2)	0.27	0.27	0.25
11/20	16.0 (±0.3)	0.5 (±0.1)	0.19	0.23	0.17	19.1 (±0.2)	1.7 (±0.3)	0.13	0.38	0.74
Site5 (low and flat)										
8/6						29.4 (±0.6)	1.5 (±0.1)	0.45	0.63	1.07
9/17	21.4 (±0.5)	0.7 (±0.1)	0.10	0.26	0.24	30.3 (±1.1)	1.1 (±0.2)	0.26	0.40	0.47
9/18	20.0 (±0.6)	0.6 (±0.1)	0.18	0.27	0.23	29.0 (±0.8)	1.0 (±0.2)	0.23	0.39	0.41

[a] Wind speeds represent the ground level values obtained with sonic anemometer measurements. Thus wind direction is strongly influenced by localized built environment, and not shown in this table. Prevailing wind direction over the urban canopy obtained from nearby weather station is presented in Table S1 in SI 3.

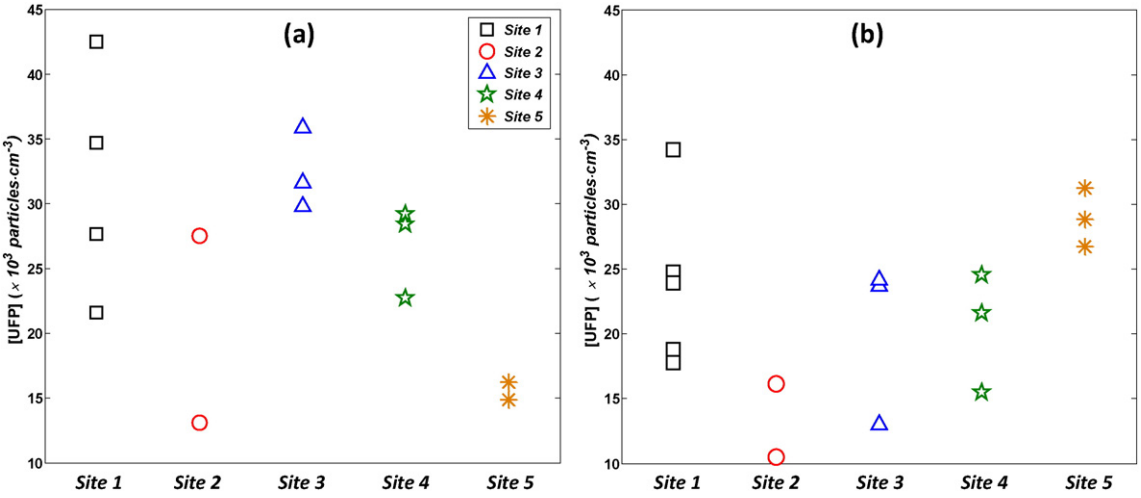

Fig. 3. Daily averaged [UFP] in the (a) morning and (b) afternoon sampling sessions at each site.

isolated tall buildings together with large open areas and/or low building areas than other sites. This heterogeneous building configuration may generate more intense turbulence near the intersections as discussed later in Section 4.3.2.

3.3. Built environments

To quantitatively investigate the built-environmental effects on street-level pollutant distributions, the key built-environmental factors were defined and calculated: the number of buildings in the sampling area; the mean building height (Eq. (1)); building area-weighted height (Eq. (2)); building heterogeneity (Eq. (3)), street width, block length, and ratio of the area occupied by buildings to the total sampling area (building density; Eq. (4)):

$$\text{Mean building height},\quad H_{bldg} = \frac{\sum_{i=1}^{N} H_i}{N} \tag{1}$$

$$\text{Building area-weighted building height},\quad H_{area} = \frac{\sum_{i=1}^{N} (S_i \times H_i)}{\sum_{i=1}^{N} S_i} \tag{2}$$

$$\text{Building heterogeneity} = H_{area}/H_{bldg}\ (1 = \text{perfectly homogeneous}) \tag{3}$$

$$\text{Building density} = \frac{\sum_{i=1}^{N} S_i}{\text{sampling area}}\ (1 = \text{entirely covered by buildings}, 0 = \text{open space}) \tag{4}$$

where, N is number of buildings in the sampling area and H_i and S_i are height and area of the i^{th} building, respectively. Sampling area is defined as the area of the rectangle covering the sampling area, as shown in Fig. 1. We note that a simple arithmetic mean of H_{bldg} can be significantly lowered when a sampling area consists of one very large isolated skyscraper and a large number of small short buildings such as *Site2* and *Site3*. Thus, we use H_{area}, which is defined as the building surface area-weighted average height (Eq. (2)). Consequently, the dimensionless ratio of H_{area} to H_{bldg} represents the building heterogeneity; this has a value of 1 for perfectly homogeneous and higher values for more heterogeneous building morphology. *Site1* and *Site5* have the most homogeneous built environments (heterogeneity of 1.16 and 1.09, respectively) but are very different: *Site1* has all tall buildings (>40 m height street canyon) and *Site5* has all small one-story buildings (lowest

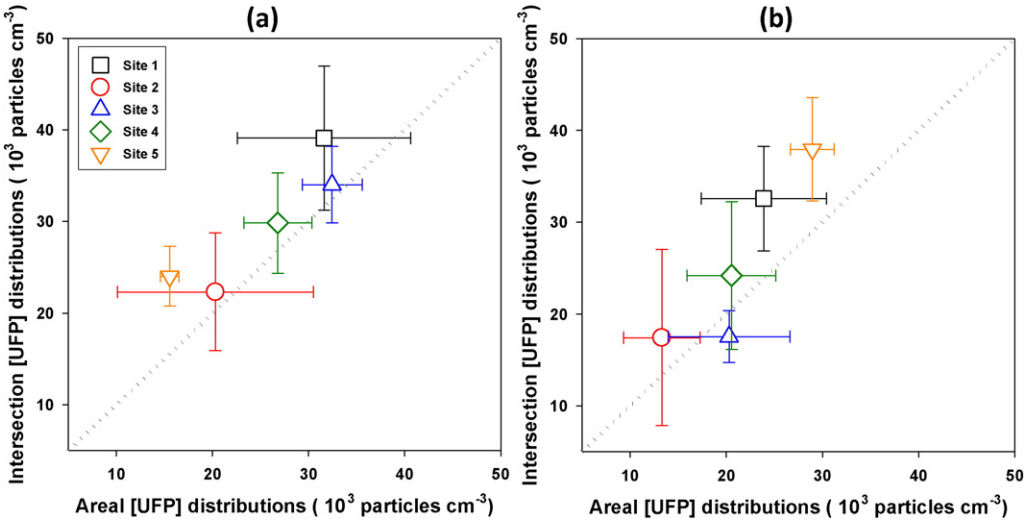

Fig. 4. The mean intersection vs. area-wide [UFP] distributions (a) in the morning and (b) afternoon sampling sessions at each site. Vertical bars denote standard deviations.

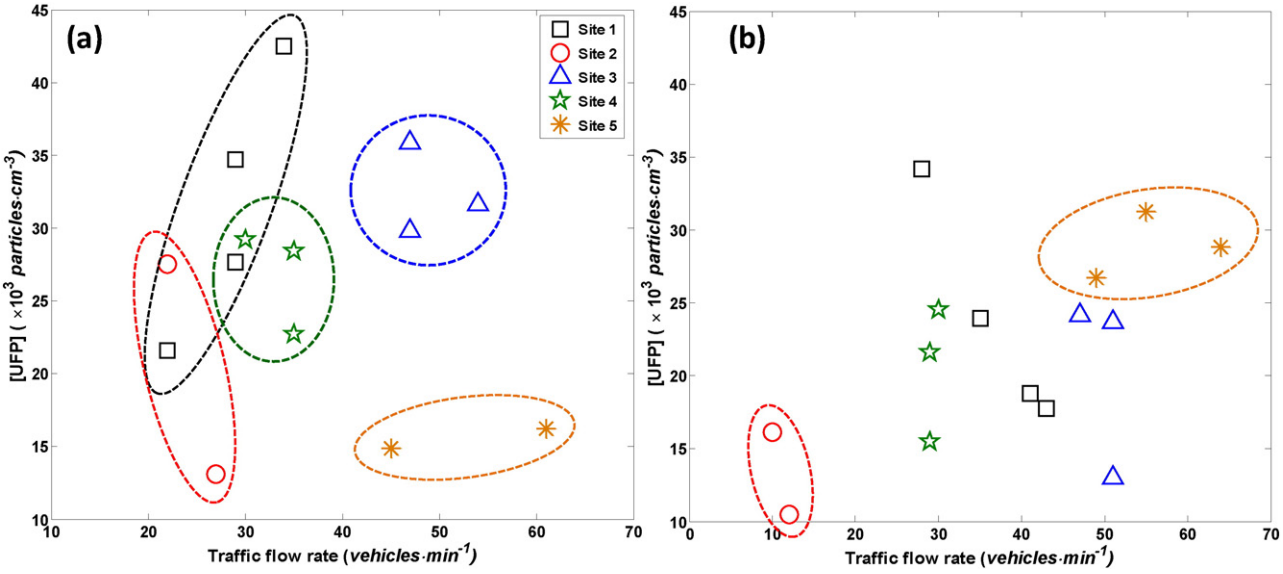

Fig. 5. Daily [UFP] as a function of traffic flow rates (vehicles·min^{-1}) in the (a) morning and (b) afternoon sampling sessions. Ovals show a group of sampling site.

building canopy of 6 m). Tall buildings on one side and small ones on the other side gave *Site4* an intermediate homogeneity of 1.39. *Site2* and *Site3* were the most heterogeneous (2.01 and 2.21, respectively). All of these quantitative parameters can be compared directly with our observed UFP concentrations to find the direct effects of built environments.

4. Results and discussions

4.1. General features of UFP concentrations

To compare the representative levels of pollutants due to roadway emissions in various built environments, concentrations obtained from mobile measurements within each sampling area were averaged. Due to significant differences in meteorology between early morning and afternoon (e.g., boundary layer depth, vertical mixing capacity, prevailing winds, and possibly secondary formation of nucleation mode particles), the morning and afternoon session results are analyzed and discussed separately.

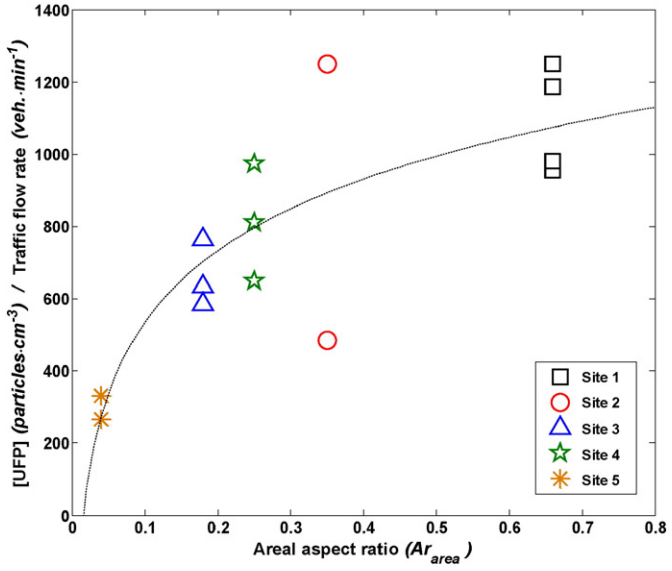

Fig. 6. Relationship between area aspect ratio (Ar_{area}) and [UFP] normalized to traffic flow rates in the morning ($R^2 = 0.67$).

Fig. 3 shows the daily mean UFP concentrations ([UFP] hereinafter) for each site. In general, [UFP] were higher in the morning than in the afternoon due to lower boundary layer heights with less turbulence, which limit vertical dispersion of emissions and increase pollutant residence time in the surface layer. Exceptions were *Site5*, *Site2* on 5 September, and *Site1* on 5 July, which showed higher concentrations in the afternoon. This cannot be explained by either emissions or dispersion because traffic rates were comparable to morning sessions and the surface atmosphere was more turbulent with a deeper boundary layer in the afternoon. The estimated boundary layer heights from vertical temperature profiles observed at Los Angeles International Airport (18 km southwest from *Site1*) were at least two times higher in the afternoon than morning sampling periods on these days: 236 m vs. 798 m on 9/5/2013; 174 m vs. 361 m on 9/17/2013; and 298 m vs. 486 m on 9/18/2013 (data on 7/5/2013 are not available).

We hypothesize that enhanced afternoon concentrations were caused by photochemical secondary production of UFP (Hu et al., 2012; Ning et al., 2007). The interesting feature is that the afternoon elevation in the transient high-spikes-removed [UFP] (see SI 5 for details) was observed only when the morning [UFP] were $<2 \times 10^4$ particles·cm^{-3}. On the other days, morning and afternoon concentrations were linearly related to one another (Fig. S8). In the morning of 5 July at *Site1*, however, $PM_{2.5}$ values were extraordinarily high (above the upper limit of DustTrak, >1 mg/m^3), presumably due to Independence Day fireworks on the evening of 4 July. Thus, lower [UFP] in the morning could be due to lower traffic (24% lower) and/or an increased coagulational sink for fresh UFP from the dramatically increased $PM_{2.5}$. *Site1*, the street canyon site in DTLA, had the highest [UFP] in both morning and afternoon, likely due to limited mixing with upper ambient air. *Site1* has a fairly homogeneous high building canopy and high simple aspect ratio, $A_r = 1.7$ (defined as the ratio of H_{area} to the mean street width, Table 2).

Site5 had the lowest [UFP] in the morning presumably due to its built environment (the lowest H_{area} and A_r, Table 2), which less inhibits vertical mixing. *Site2* also had low [UFP] compared to the other sites, even though the simple A_r at this site is highest ($A_r = 1.9$). This can be explained by relatively low traffic rates at this site, combined with a negligible number of vehicles in queues during red lights. We also note that the simple A_r does not account for open spaces (e.g. the gaps between buildings or large parking lots). The high A_r at *Site2* derives from two tall isolated skyscrapers but this site also has vast open parking areas (Fig. S2), as shown by the minimal number of buildings in the selected area (Table 2). Morning [UFP] at *Site3* were comparable

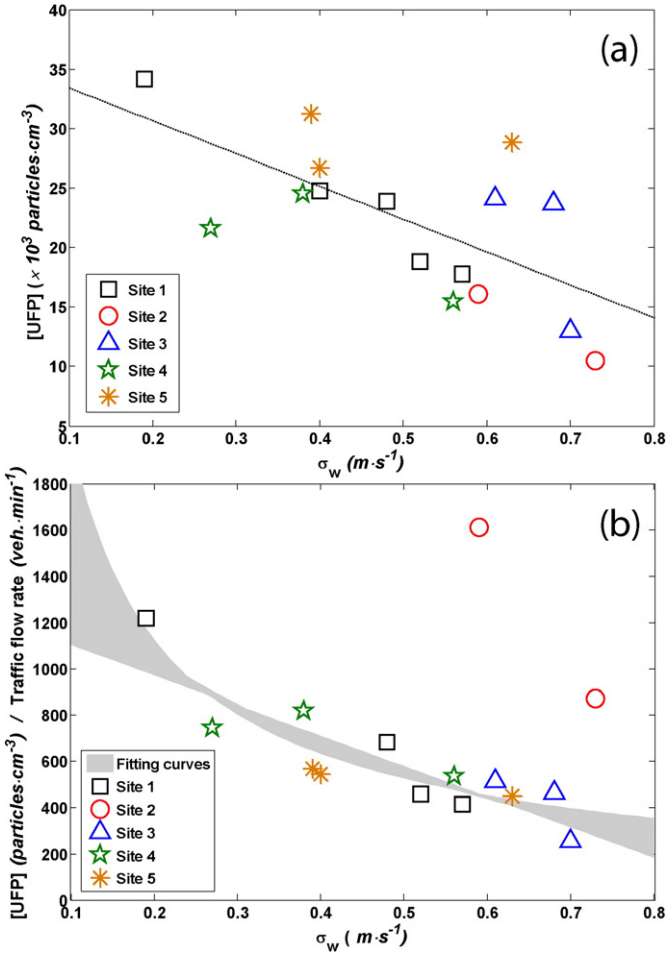

Fig. 7. Relationship between [UFP] and σ_w for afternoon sessions. (a) [UFP] vs. σ_w and (b) [UFP] normalized by observed traffic flows vs. σ_w. The gray area represents the range of best fit curves as described in the text. The values for *Site2* are excepted from the analysis due to very low traffic counts on the street and subsequent likely contributions from nearby streets and other sources (see text).

to *Site1* but sharply decreased in the afternoon, reaching levels similar to *Site4* and lower than *Site1*. The elevated concentrations in the morning at *Site3* were likely due to both the heavy traffic flows and density (Table 3). However, given that traffic rate and density at *Site3* were similar between morning and afternoon sessions and higher than those at *Site1* and *Site4*, lowered afternoon [UFP] compared to *Site1* and *Site4* cannot be readily explained. Consequently, these observations strongly suggest that [UFP] for each site are controlled by different factors depending on meteorological and built-environmental conditions. Quantitative discussions concerning factors controlling the UFP levels in various environments are presented in Section 4.3.

4.2. Elevated emissions at the intersections

One of the objectives of this field study was to investigate variations in [UFP] from roadway emissions in the close vicinity of pedestrian walkways (thus, closely reflecting pedestrian exposure) in various micro-built environments. In this respect, we present general quantitative impacts of vehicle acceleration at intersections. Fig. 4 shows the session mean [UFP] at intersection corners (measured with stationary DiSCminis) vs. the average for the whole sampling area (measured with the MMP). The intersection averages were consistently higher than the whole sampling area average in both morning and afternoon sessions for all sites except *Site3* afternoon sessions. In the morning, [UFP] at the intersections was higher than the sampling area average by 24%, 10%, 5%, 11% and 55% at *Site1*, *Site2*, *Site3*, *Site4* and *Site5*, respectively; in the afternoon, intersections corners were higher by 36%, 31%, −14%, 18% and 31%, respectively. Traffic at *Site3* was concentrated on Vermont Ave. and, due to a long queue that covered the entire sampling blocks, acceleration events were limited and occurred over the whole sampling section of Vermont Ave., likely causing less significant intersection impacts.

Consistently higher [UFP] at the corners of intersections provides clear evidence that acceleration of vehicles at intersections increases pedestrian exposure to UFP. This is consistent with the argument in Klems et al. (2010) that the dominant period of transient spikes in UFP time-series matches traffic-light cycles. Although Klems et al. (2010) addressed only occurrences and periods of spikes from the intersection accelerations, we additionally observed that the spike-removed baseline levels obtained with the same method in Choi et al. (2013) (and

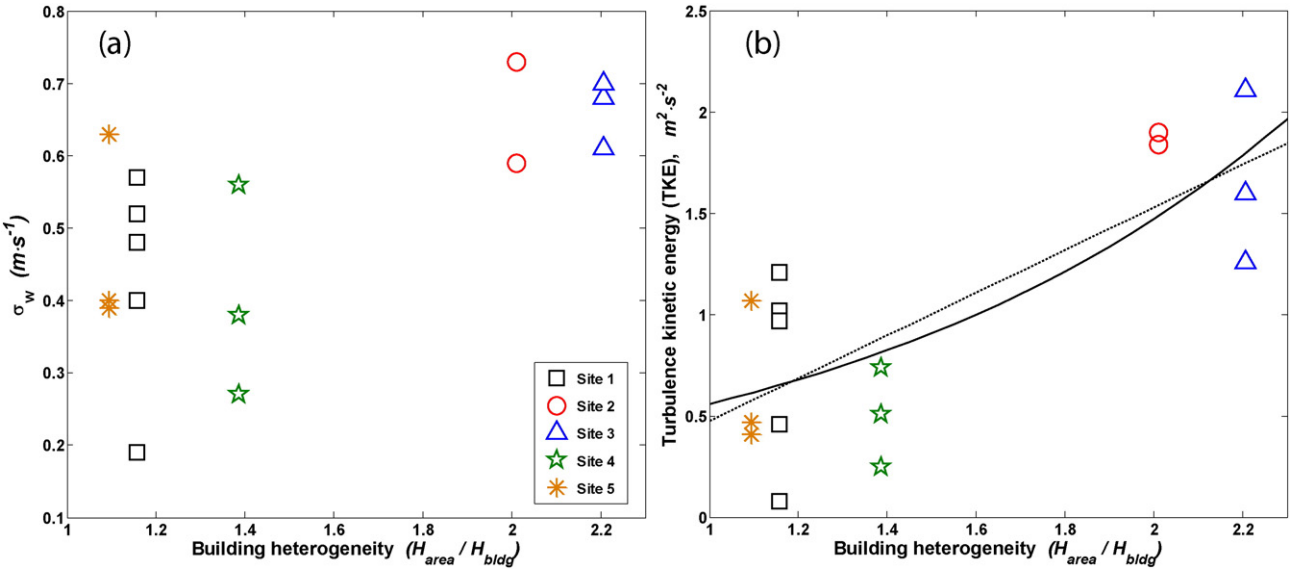

Fig. 8. Afternoon relationships between building heterogeneity vs. turbulence intensities: (a) vertical fluctuation of winds and (b) total turbulence kinetic energy (TKE) defined as $TKE = 1/2\sqrt{\sigma_u^2 + \sigma_v^2 + \sigma_w^2}$. Dotted and solid lines in (b) represent the best fits in linear ($R^2 = 0.60$) and exponential ($R^2 = 0.60$) forms, respectively, for illustration of the increase trends of TKE with building heterogeneity.

Table 5
Summary for planners: Built environment and traffic management design characteristics that influence near-roadway exposures to vehicular pollution.

Management	Suggested direction	Approx. size of effect	Atmospheric conditions& notes
Areal aspect ratio (A_{area}) A_{area} combines building area-weighted height, building footprint, and the amount of open space.	Lower building volumes and more open space result in lower pollutant concentrations.	Up to approximately a factor of three.	Important under calm conditions (in the mornings at our sites). Not critical when the atmosphere is unstable.
Building heterogeneity	Isolated tall buildings result in lower concentrations than homogeneous shorter or higher buildings with similar volume.	Up to approximately a factor of two.	Important under unstable conditions with moderate winds (afternoons at our sites). Not critical when the atmosphere is stable.
Traffic flow	Lower traffic flow is better, controlling for fleet mix.	At a given location, concentrations are roughly proportional to traffic flow.	
Traffic management	Fewer stops and smaller queues reduce emissions and elevated concentrations around intersections	Cannot estimate from our data	Concentrations depend on emissions, micro-scale turbulence, dispersion, transport from nearby streets, and other factors

described briefly in SI 5) were higher also at intersection corners compared to the values over the sampling area: 29/33%, 15/38%, 2/3%, 7/18%, and 61/27% for *Sites1*, *Site2*, *Site3*, *Site4*, and *Site5* in the morning/afternoon, respectively (Fig. S9). This implies, perhaps unsurprisingly, that higher emissions from vehicle accelerations at intersections are quickly mixed with ambient air and, at steady-state, result in persistently higher [UFP] in the intersection areas.

Given that the MMP route includes intersection areas (Fig. 1) and the peak concentrations due to acceleration do not necessarily appear exactly at the corners (they can instead appear before and/or after intersections) (Ranasinghe et al., 2016), the concentration difference at intersection vs. over the sampling area can be higher than the values presented above. More complete analyses for the intersection impacts (including the locations and shapes of intersection peaks) will be presented separately.

4.3. Factors controlling near-roadway UFP concentrations

4.3.1. Calm morning conditions

Most morning sampling periods were calm, and meteorological variations between sites were not sufficient to explain the wide [UFP] variations among sites (Fig. SI 7). Traffic differences were noticeable between sites, but day-to-day variations at a single site were relatively insignificant. It appears that, in general, higher traffic rates led to higher levels of UFP, except at the two sites with extreme built-environments: the street canyon (*Site1*) and the low, flat canopy (*Site5*). The homogeneous high building canopy in the street canyon had higher [UFP] compared to observed traffic flow rates, and the opposite was true for the homogeneous and lowest building canopy (Fig. 5a).

A noticeable positive correlation was found between [UFP] and building area-weighted building height H_{area}, particularly in the morning (Fig. S10 in SI 6). *Site1* and *Site2* have similar H_{area} values of around 40 m, however, the high H_{area} at *Site2* results from few very tall buildings (~130 m) on a site with many large open parking lots around the intersection (Table 2 and Fig. S2a), while *Site1* is largely surrounded by ~40 m buildings. To better capture the different built-environmental characteristics, a block-scale areal aspect ratio (Ar_{area}) was developed (Eq. (5)):

$$Ar_{area} = \frac{H_{area}}{L_{diag} \times \left(1 - \sum S_{bldg}/A_{site}\right)} = \frac{H_{area}}{L_{diag} \times \left(A_{open}/A_{site}\right)} = \frac{H_{area}}{L_{open}} \quad (5)$$

where $\sum S_{bldg}$ is the sum of the building ground areas, A_{site} is the area of the sampling site, L_{diag} is the diagonal block length, and L_{open} and A_{open} are the length scale and area of open space, respectively.

The traffic-corrected [UFP], which is defined simply as observed [UFP] divided by observed traffic flow rate, showed a strong relationship with Ar_{area} (Fig. 6 and Eq. (6)):

$$\frac{[\text{UFP}]}{\text{Traffic flow rate}} = 286 \times \log(Ar_{area}) + 1193 \quad \left(R^2 = 0.67\right). \quad (6)$$

Due to a log form of the best fit curve, [UFP] increase sharply with Ar_{area} in a low Ar_{area} regime, but in a high Ar_{area} regime, the slope of [UFP] elevation with Ar_{area} is dampened. The log form of the best fit implies that once the aspect ratio is above a critical level, recirculation cells form in the lower part of building canopy (Liu et al., 2004). Once the in-canopy recirculation cells are a dominant feature, additional increases in aspect ratio have a weaker effect on ground-level vehicular pollutants because recirculation cells separate ground-level in-canopy air from upper ambient air. More details about air flow impacts on spatial distributions of pollutants will be presented in a separate study (Ranasinghe et al., 2016). Consequently, our results suggest that built environments, particularly the areal aspect ratio (Ar_{area}) and traffic conditions, determine the spatial patterns of UFP levels under calm morning conditions.

4.3.2. Unstable afternoon conditions

The areal aspect ratio does not explain the afternoon [UFP] between sites as well as it does for morning distributions (Fig. S10). This is not surprising given an increasing meteorological influence due to more diverse meteorology between sites/days in the afternoon, such as deeper boundary layer depth and stronger turbulence intensities (Choi et al., 2011; Hussein et al., 2006; Seibert et al., 2000), as well as the additional possible UFP source of photochemical secondary production (Hu et al., 2012; Ning et al., 2007).

In the afternoon, vertical fluctuations of winds (σ_w) are the strongest factor in determining UFP levels, as shown by the straightforward relationships between [UFP] and σ_w ($R^2 = 0.43$, Fig. 7a). As the surface atmosphere becomes more turbulent (higher σ_w), UFP levels decrease due to stronger atmospheric dispersion. The effect of σ_w on [UFP] becomes more evident when [UFP] are corrected by traffic flow rate; R^2 values increase up to 0.83 (Fig. 7b). Note that two data points obtained from *Site2* clearly departed from the trend and thus were excluded from the curve fitting analyses. *Site2* has very infrequent traffic with traffic flow rates of only 1/3 to 1/5 that of other sites (Table 2). Relatively high [UFP] despite minimal vehicular emissions at this site are likely caused by an influx from nearby busy streets combined with a contribution from secondary production (Brines et al., 2015). This implies that an understanding of horizontal wind fields is required to understand the heterogeneous spatial distributions of pollutants, particularly on streets with little pollution of their own.

There is not an obvious theoretical basis from which to derive a quantitative relationship between σ_w and traffic normalized [UFP], and our data do not span a large enough range to suggest the best form. Thus, several types of simple curve fits were applied: linear, exponential, logarithmic, and power (Eq. (7)). The linear form resulted in slightly lower R^2 value compared to others. Although the fitted values disperse widely at the both ends, all fits showed a good agreement within observed σ_w range; the shaded area in Fig. 7b shows the maximum and minimum values of the curve fits.

$$\frac{\text{PNC}}{\text{Traffic flow rate}} = \begin{cases} -1315 \cdot \sigma_w + 1236 & \left(R^2 = 0.74\right) \\ 1645 \cdot \exp(-2.21 \cdot \sigma_w) & \left(R^2 = 0.80\right) \\ -563 \cdot \log(0.76 \cdot \sigma_w) & \left(R^2 = 0.81\right) \\ 296 \cdot {\sigma_w}^{-0.83} & \left(R^2 = 0.83\right) \end{cases} \quad (7)$$

The strong relationships between traffic-normalized [UFP] and σ_w emphasize the role of surface micrometeorology in determining afternoon pollutant levels. However, we hypothesize that built environments also affect pollutant distributions indirectly by altering the strength of turbulence intensities. To support this hypothesis, the comparisons between heterogeneity of building morphology for each site and observed surface turbulence parameters are shown in Fig. 8.

The fluctuations of vertical winds that showed the strongest relationships with the afternoon [UFP] appear to be somewhat related to building heterogeneity (Fig. 8a). However, the daily variations of σ_w for each site are so large compared to the magnitude of the observed range that the relationships are not so strong. On the other hand, it is clear that the most heterogeneous sites, *Site2* and *Site3*, had consistently stronger σ_w than other more homogeneous sites. Indeed, the surface level turbulence kinetic energy for each site sharply increased with building heterogeneity (Fig. 8b). This relationship implies that a heterogeneous building configuration enhances surface level turbulence, intensifying atmospheric dispersive capacity and reducing surface pollutant levels under unstable daytime conditions.

5. Implications for urban planners and traffic managers

Our research findings have implications for urban planning, traffic management policies and air pollution exposure of pedestrians and vehicle occupants in urban centers. Broadly, our data provide quantitative insights into how the built environment and traffic flows influence pedestrian exposure to vehicle pollution, and offer urban planners and traffic managers strategies to reduce street level pollutant concentrations.

Table 5 summarizes built environment and traffic management design characteristics at the block scale that influence near-roadway exposures to vehicle pollution. Our findings that lower traffic flows and fewer stops reduce near-roadway pollution are consistent with earlier studies and enlightened traffic management policies. In addition to the obvious dependence on traffic volumes, different built environment characteristics are important at different atmospheric stability/times of the day. For calm mornings, the area aspect ratio (Ar_{area}) was an important factor in controlling the block-scale vehicular pollutant concentrations. Higher values of Ar_{area}, correspond to more building volume and less open space, and limited mixing with ambient air above. On the other hand, turbulence intensities, represented by σ_w, played a major role in dispersing vehicular emissions in the afternoon. The built environment affects surface turbulence intensities, and thus plays an indirect role in controlling block-scale [UFP]. An isolated tall building surrounded by open space or short buildings is likely help to reduce the levels of vehicular pollution by increasing surface level turbulence intensities. Thus, urban planning focused on decreasing Ar_{area} and increasing heterogeneity of building distributions is expected to substantially improve near-roadway air quality and reduce pedestrian exposure to vehicular emissions.

Acknowledgements

The authors gratefully acknowledge support for this study by the California Air Resources Board, Contract No. 12-308 and U.S. National Science Foundation, Contract No. CNS-1111971001. The first author was partially funded by Korean Ministry of Environment through "Climate Change Correspondence Program". The mobile monitoring platform measurements were made possible with the generous assistance of our colleagues Kathleen Kozawa and Steve Mara. The authors also appreciate Prof. A. Venkatram, Mr. Schulte, and Dr. S. Tan at the University of California, Riverside for the sonic anemometer data. The views and opinions in this study are those of the authors and do not reflect the official views of the CARB.

Appendix A. Supplementary data

Supplementary data to this article can be found online at http://dx.doi.org/10.1016/j.scitotenv.2016.02.083.

References

Bau, S., Zimmermann, B., Payet, R., Witschger, O., 2015. A laboratory study of the performance of the handheld diffusion size classifier (DiSCmini) for various aerosols in the 15–400 nm range. Environ. Sci. Process. Impacts. http://dx.doi.org/10.1039/c1034em00491d (Advance Article).

Behrentz, E., Sabin, L.D., Winer, A.M., Fitz, D.R., Pankratz, D.V., Colome, S.D., Fruin, S.A., 2005. Relative importance of school bus-related microenvironments to children's pollutant exposure. J. Air Waste Manage. Assoc. 55, 1418–1430.

Boarnet, M.G., Houston, D., Edwards, R., Princevac, M., Ferguson, G., Pan, H.S., Bartolome, C., 2011. Fine particulate concentrations on sidewalks in five Southern California cities. Atmos. Environ. 45, 4025–4033.

Boogaard, H., Kos, G.P.A., Weijers, E.P., Janssen, N.A.H., Fischer, P.H., van der Zee, S.C., de Hartog, J.J., Hoek, G., 2011. Contrast in air pollution components between major streets and background locations: particulate matter mass, black carbon, elemental composition, nitrogen oxide and ultrafine particle number. Atmos. Environ. 45, 650–658.

Brines, M., Dall'Osto, M., Beddows, D.C.S., Harrison, R.M., Gomez-Moreno, F., Nunez, L., Artinano, B., Costabile, F., Gobbi, G.P., Salimi, F., Morawska, L., Sioutas, C., Querol, X., 2015. Traffic and nucleation events as main sources of ultrafine particles in high-insolation developed world cities. Atmos. Chem. Phys. 15, 5929–5945.

Brugge, D., Durant, J.L., Rioux, C., 2007. Near-highway pollutants in motor vehicle exhaust: a review of epidemiologic evidence of cardiac and pulmonary health risks. Environ. Heal. 6, 12.

Buonanno, G., Fuoco, F.C., Stabile, L., 2011. Influential parameters on particle exposure of pedestrians in urban microenvironments. Atmos. Environ. 45, 1434–1443.

Capaldo, K., Pandis, S., 2001. Lifetimes of Ultrafine Diesel Aerosol, Report for the University of Minnesota and the Coordinating Research Council under the E-43 Project Diesel Aerosol Sampling Methodology. Carnegie Mellon University, Pittsburgh, PA.

Choi, W., Faloona, I.C., McKay, M., Goldstein, A.H., Baker, B., 2011. Estimating the atmospheric boundary layer height over sloped, forested terrain from surface spectral analysis during BEARPEX. Atmos. Chem. Phys. 11, 6837–6853.

Choi, W., He, M., Barbesant, V., Kozawa, K.H., Mara, S., Winer, A.M., Paulson, S.E., 2012. Prevalence of wide area impacts downwind freeways under pre-sunrise stable atmospheric conditions. Atmos. Environ. 62, 318–327.

Choi, W., Hu, S.S., He, M., Kozawa, K.H., Mara, S., Winer, A.M., Paulson, S.E., 2013. Neighborhood-scale air quality impacts of emissions from motor vehicles and aircraft. Atmos. Environ. 80, 310–321.

Fruin, S.A., Winer, A.M., Rodes, C.E., 2004. Black carbon concentrations in California vehicles and estimation of in-vehicle diesel exhaust particulate matter exposures. Atmos. Environ. 38, 4123–4133.

Haughey, R., Sherriff, R., 2010. Challenges and Policy Options for Creating and Preserving Affordable Housing Near Transit and Other Location-efficient Areas. Center for Housing Policy.

Hoek, G., Brunekreef, B., Goldbohm, S., Fischer, P., van den Brandt, P.A., 2002. Association between mortality and indicators of traffic-related air pollution in the Netherlands: a cohort study. Lancet 360, 1203–1209.

Hu, S., Paulson, S.E., Fruin, S., Kozawa, K., Mara, S., Winer, A.M., 2012. Observation of elevated air pollutant concentrations in a residential neighborhood of Los Angeles California using a mobile platform. Atmos. Environ. 51, 311–319.

Hussein, T., Karppinen, A., Kukkonen, J., Harkonen, J., Aalto, P.P., Hameri, K., Kerminen, V.M., Kulmala, M., 2006. Meteorological dependence of size-fractionated number concentrations of urban aerosol particles. Atmos. Environ. 40, 1427–1440.

Janssen, N.A.H., Brunekreef, B., van Vliet, P., Aarts, F., Meliefste, K., Harssema, H., Fischer, P., 2003. The relationship between air pollution from heavy traffic and allergic sensitization, bronchial hyperresponsiveness, and respiratory symptoms in Dutch schoolchildren. Environ. Health Perspect. 111, 1512–1518.

Klems, J.P., Pennington, M.R., Zordan, C.A., Johnston, M.V., 2010. Ultrafine particles near a roadway intersection: origin and apportionment of fast changes in concentration. Environ. Sci. Technol. 44, 7903–7907.
Kozawa, K.H., Fruin, S.A., Winer, A.M., 2009. Near-road air pollution impacts of goods movement in communities adjacent to the ports of Los Angeles and Long Beach. Atmos. Environ. 43, 2960–2970.
LARIAC, 2009. Los Angeles Region Imagery Acuisition Consortium (LARIAC) Data Archives. Los Angeles County GIS Data Portal, Los Angeles.
Liu, C.-H., Barth, M.C., Leung, D.Y.C., 2004. Large-Eddy simulation of flow and pollutant transport in street canyons of different building-height–street-width ratios. J. Appl. Meteorol. 43, 1410–1424.
Marshall, J.D., McKone, T.E., Deakin, E., Nazaroff, W.W., 2005. Inhalation of motor vehicle emissions: effects of urban population and land area. Atmos. Environ. 39, 283–295.
Mills, J.B., Park, J.H., Peters, T.M., 2013. Comparison of the DiSCmini aerosol monitor to a handheld Condensation Particle Counter and a Scanning Mobility Particle Sizer for submicrometer sodium chloride and metal aerosols. J. Occup. Environ. Hyg. 10, 250–258.
Morawska, L., Ristovski, Z., Jayaratne, E.R., Keogh, D.U., Ling, X., 2008. Ambient nano and ultrafine particles from motor vehicle emissions: characteristics, ambient processing and implications on human exposure. Atmos. Environ. 42, 8113–8138.
Ning, Z., Geller, M.D., Moore, K.F., Sheesley, R., Schauer, J.J., Sioutas, C., 2007. Daily variation in chemical characterisitics of urban ultrafine aerosols and inference of their sources. Environ. Sci. Technol. 41, 6000–6006.
Pearson, R.L., Wachtel, H., Ebi, K.L., 2000. Distance-weighted traffic density in proximity to a home is a risk factor for leukemia and other childhood cancers. J. Air Waste Manage. Assoc. 50, 175–180.
Pirjola, L., Lähde, T., Niemi, J.V., Kousa, A., Rönkkö, T., Karjalainen, P., Keskinen, J., Frey, A., Hillamo, R., 2012. Spatial and temporal characterization of traffic emissions in urban microenvironments with a mobile laboratory. Atmos. Environ. 63, 156–167.
Ranasinghe, D., Choi, W., Winer, A.M., Paulson, S.E., 2016. Developing high spatial resolution concentration maps using mobile air quality measurements. Aerosol and Air Quality Research (under review).
Ren, C., Wu, J., Chung, J.H., Delfino, R.J., Ritz, B., 2008. Association between local traffic-generated air pollution and preterm delivery in the South Coast Air Basin of California. Epidemiology 19, S158–S159.
Seibert, P., Beyrich, F., Gryning, S.E., Joffre, S., Rasmussen, A., Tercier, P., 2000. Review and intercomparison of operational methods for the determination of the mixing height. Atmos. Environ. 34, 1001–1027.
Tonne, C., Melly, S., Mittleman, M., Coull, B., Goldberg, R., Schwartz, J., 2007. A case–control analysis of exposure to traffic and acute myocardial infarction. Environ. Health Perspect. 115, 53–57.
Volk, H.E., Hertz-Picciotto, I., Delwiche, L., Lurmann, F., McConnell, R., 2011. Residential proximity to freeways and autism in the CHARGE study. Environ. Health Perspect. 119, 873–877.
Zhou, Y., Levy, J.I., 2007. Factors influencing the spatial extent of mobile source air pollution impacts: a meta-analysis. BMC Public Health 7.